

DISTRIBUTED ALLOCATION OF MOBILE SENSING SWARMS IN GYRE FLOWS

KENNETH MALLORY and M. ANI HSIEH¹, ERIC FORGOSTON², and IRA B. SCHWARTZ³

¹SAS LAB, DREXEL UNIVERSITY, PHILADELPHIA, PA 19104, USA

²DEPARTMENT OF MATHEMATICAL SCIENCES, MONTCLAIR STATE UNIVERSITY, MONTCLAIR, NJ 07043, USA

³NONLINEAR SYSTEMS DYNAMICS SECTION, PLASMA PHYSICS DIVISION, CODE 6792, U.S. NAVAL RESEARCH LAB, WASHINGTON, DC 20375, USA

Correspondence to: KENNETH MALLORY
(km374@drexel.edu)

Abstract. We address the synthesis of distributed control policies to enable a swarm of homogeneous mobile sensors to maintain a desired spatial distribution in a geophysical flow environment, or workspace. In this article, we assume the mobile sensors (or robots) have a “map” of the environment denoting the locations of the Lagrangian coherent structures or LCS boundaries. Based on this information, we design agent-level hybrid control policies that leverage the surrounding fluid dynamics and inherent environmental noise to enable the team to maintain a desired distribution in the workspace. We establish the stability properties of the ensemble dynamics of the distributed control policies. Since realistic quasi-geostrophic ocean models predict double-gyre flow solutions, we use a wind-driven multi-gyre flow model to verify the feasibility of the proposed distributed control strategy and compare the proposed control strategy with a baseline deterministic allocation strategy. Lastly, we validate the control strategy using actual flow data obtained by our coherent structure experimental testbed.

mostly focused on the deployment of single, or small numbers of, AUVs working in conjunction with a few stationary sensors and ASVs. While data collection strategies in these works are driven by the dynamics of the processes they study, few existing approaches explicitly account for the surrounding fluid dynamics (Lolla et al., 2012; DeVries and Paley, 2011). In fact, most existing works treat the effect of the surrounding fluid as external disturbances (Das et al., 2011; Williams and Sukhatme, 2012), largely because of our limited understanding of the complexities of ocean dynamics.

Geophysical flows are naturally stochastic and aperiodic, yet exhibit coherent structure. Coherent structures are of significant importance since knowledge of them enables the prediction and estimation of the underlying geophysical fluid dynamics. In realistic ocean flows, these time-dependent coherent structures, or Lagrangian coherent structures (LCS), are similar to separatrices that divide the flow into dynamically distinct regions. LCS are extensions of stable and unstable manifolds to general time-dependent flows (Haller and Yuan, 2000), and they carry a great deal of global information about the dynamics of the flows. For two-dimensional (2D) flows, ridges of locally maximal finite-time Lyapunov exponent (FTLE) (Shadden et al., 2005) values correspond, to a good approximation (though see (Haller, 2011)), to Lagrangian coherent structures. LCS have been shown to coincide with optimal trajectories in the ocean which minimize the energy and the time needed to traverse from one point to another (Inanc et al., 2005; Senatore and Ross, 2008). Furthermore, for monitoring of oceanic processes, *e.g.*, to improve weather and climate forecasting or to better understand contaminant transport, one would like to use autonomous

1 Introduction

Recent years have seen the use of autonomous underwater and surface vehicles (AUVs and ASVs) for persistent surveillance of the ocean to study the dynamics of various biological and physical phenomena, such as plankton assemblages (Caron et al., 2008), temperature and salinity profiles (Lynch et al., 2008; Wu and Zhang, 2011; Sydney and Paley, 2011), and the onset of harmful algae blooms (Zhang et al., 2007; Chen et al., 2008; Das et al., 2011). These studies have

sensors to measure a variety of quantities of interest. A drawback to operating sensors in time-dependent and stochastic environments like the ocean is that the sensors will escape from their monitoring region of interest with some finite probability. Since the LCS are inherently unstable and denote regions of the flow where escape events occur with higher probability (Forgoston et al., 2011), knowledge of the LCS are of paramount importance in maintaining a sensor in a particular monitoring region.

Recently, Hsieh et al. (2012) described a collaborative control strategy for a class of autonomous underwater vehicles (AUVs) to track the coherent structures and manifolds on flows. In this paper, we now present a distributed control strategy for AUVs and/or mobile sensing resources to maintain a desired spatial distribution assuming *a priori* knowledge of manifold/coherent structure locations within a region of interest. Specifically, we devise agent-level control policies which allow individual AUVs to leverage the surrounding fluid dynamics and inherent environmental noise to navigate from one dynamically distinct region to another in a fluidic environment. The result is a distributed allocation strategy that minimizes the overall control-effort employed by the team to maintain the desired spatial formation for environmental monitoring applications. While this problem can be formulated as a multi-task (MT), single-robot (SR), time-extended assignment (TA) problem (Gerkey and Mataric, 2004), existing approaches do not take into account the effects of fluid dynamics coupled with the inherent environmental noise (Gerkey and Mataric, 2002; Dias et al., 2006; Dahl et al., 2006; Hsieh et al., 2008; Berman et al., 2008). As such, the novelty of this work lies in the use of nonlinear dynamical systems tools and recent results in distributed robotic tracking of manifolds and structures (Hsieh et al., 2012) to synthesize distributed control policies that enables agents to maintain a desired distribution in a fluidic environment.

The paper is structured as follows: We formulate the problem and outline key assumptions in Section 2. The development of the distributed control strategy is presented in Section 3 and its theoretical properties are analyzed in Section 4. Section 5 presents our simulation methodology and results. We conclude with a discussion of our results, and directions for future work in Sections 6 and 7 respectively.

2 Problem Formulation

Consider the deployment of N mobile sensing resources (AUVs/ASVs) to monitor M regions in the ocean. The objective is to synthesize agent-level control policies that will enable the team to autonomously maintain a desired distribution across the M regions in a dynamic and noisy fluidic environment. We assume the following kinematic model for each AUV:

$$\dot{\mathbf{q}}_k = \mathbf{u}_k + \mathbf{v}_f(\mathbf{q}_k) \quad k \in \{1, \dots, n\}, \quad (1)$$

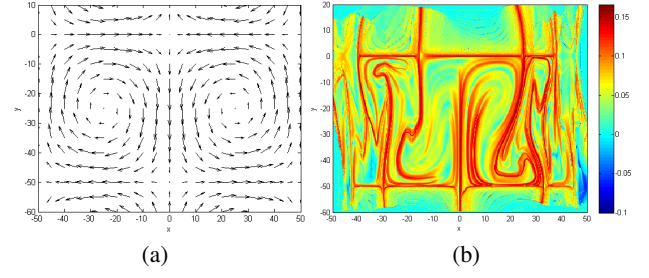


Fig. 1. (a) Vector field and (b) FTLE field of the model given by (2) for two gyres with $A = 10$, $\mu = 0.005$, $\varepsilon = 0$, $\psi = 0$, $I = 0.01$, and $s = 50$. LCS are characterized by regions with maximum FTLE measures (denoted by red). In 2D flows, regions with maximum FTLE measures correspond to 1-D curves.

where $\mathbf{q}_k = [x_k, y_k, z_k]^T$ denotes the vehicle's position, \mathbf{u}_k denotes the 3×1 control input vector, and $\mathbf{v}_f(\mathbf{q}_k)$ denotes the velocity of the fluid experienced/measured by the k^{th} vehicle.

In this article, we limit our discussion to 2D planar flows and motions and thus we assume z_k is constant for all k . As such, $\mathbf{v}_f(\mathbf{q})$ is given by a 2D vector field denoted by $F(\mathbf{q})$ such that $F_z(\mathbf{q}) = 0$ for all \mathbf{q} . Since realistic quasi-geostrophic ocean models exhibit multi-gyre flow solutions, we assume $\mathbf{v}_f(\mathbf{q}) = F(\mathbf{q})$ where $F(\mathbf{q})$ is provided by the 2D wind-driven multi-gyre flow model given by

$$\dot{x} = -\pi A \sin\left(\pi \frac{f(x,t)}{s}\right) \cos\left(\pi \frac{y}{s}\right) - \mu x + \eta_1(t), \quad (2a)$$

$$\dot{y} = \pi A \cos\left(\pi \frac{f(x,t)}{s}\right) \sin\left(\pi \frac{y}{s}\right) \frac{df}{dx} - \mu y + \eta_2(t), \quad (2b)$$

$$\dot{z} = 0, \quad (2c)$$

$$f(x,t) = x + \varepsilon \sin\left(\pi \frac{x + \phi}{\rho}\right) \sin(\omega t + \psi). \quad (2d)$$

When $\varepsilon = 0$, the multi-gyre flow is time-independent, while for $\varepsilon \neq 0$, the gyres undergo a periodic expansion and contraction in the x direction. In Eq. (2), A approximately determines the amplitude of the velocity vectors, $\omega/2\pi$ gives the oscillation frequency, ε determines the amplitude of the left-right motion of the separatrix between the gyres, ψ is the phase, μ determines the dissipation, s scales the dimensions of the workspace, and $\eta_i(t)$ describes a stochastic white noise with mean zero and standard deviation $\sigma = \sqrt{2I}$, for noise intensity I . Figs. 1(a) and 1(b) show the vector field of a two-gyre model and the corresponding FTLE curves for the time independent case.

Let \mathcal{W} denote an obstacle-free workspace with flow dynamics given by (2). We assume a tessellation of \mathcal{W} such that the boundaries of each cell roughly corresponds to stable/unstable manifolds or LCS curves quantified by maximum FTLE ridges as shown in Fig. 2. A tessellation of the workspace along boundaries characterized by maximum FTLE ridges makes sense since they separate regions within

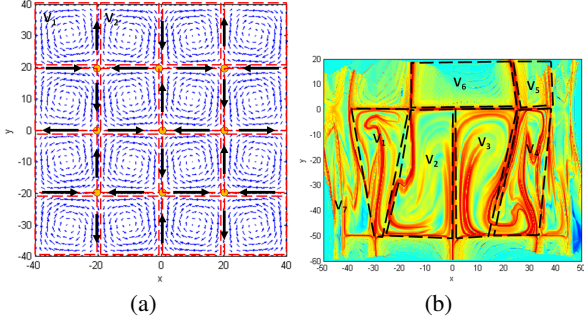


Fig. 2. Two examples of cell decomposition of the region of interest based on (2). (a) A 4×4 time independent grid of gyres with $A = 0.5$, $\mu = 0.005$, $\varepsilon = 0$, $\psi = 0$, $I = 35$, and $s = 20$. The stable and unstable manifolds of each saddle point in the system is shown by the black arrows. (b) An FTLE based cell decomposition for a time-independent double-gyre system with the same parameters as Fig. 1(b).

the flow field that exhibit distinct dynamic behavior and denote regions in the flow field where more escape events may occur probabilistically (Forgoston et al., 2011). In the time independent case, these boundaries correspond to stable and unstable manifolds of saddle points in the system. The manifolds can also be characterized by maximum FTLE ridges where the FTLE is computed based on a backward (attracting structures) or forward (repelling structures) integration in time. Since the manifolds demarcate the basin boundaries separating the distinct dynamical regions, they are also regions that are uncertain with respect to velocity vectors within a neighborhood of the manifold. Therefore, switching between regions in neighborhoods of the manifold is influenced both by deterministic uncertainty as well as stochasticity due to external noise.

Given an FTLE-based cell decomposition of \mathcal{W} , let $\mathcal{G} = (\mathcal{V}, \mathcal{E})$ denote an undirected graph whose vertex set $\mathcal{V} = \{V_1, \dots, V_M\}$ represents the collection of FTLE-derived cells in \mathcal{W} . An edge e_{ij} exists in the set \mathcal{E} if cells V_i and V_j share a physical boundary or are physically adjacent. In other words, \mathcal{G} serves as a roadmap for \mathcal{W} . For the case shown in Fig. 2(a), adjacency of an interior cell is defined based on four neighborhoods. Let N_i denote the number of AUVs or mobile sensing resources/robots within V_i . The objective is to synthesize agent-level control policies, or \mathbf{u}_k , to achieve and maintain a desired distribution of the N agents across the M regions, denoted by $\tilde{\mathbf{N}} = [\tilde{N}_1, \dots, \tilde{N}_M]^T$, in an environment whose dynamics are given by (2).

We assume that robots are given a map of the environment, \mathcal{G} , know the locations of the LCS boundaries for each V_i , have the ability to communicate with other robots collocated within the same V_i , and $\tilde{\mathbf{N}}$ is known *a priori*. These assumptions are necessary to enable a prioritization scheme within each V_i based on an individual robot's escape likelihoods in order to achieve the desired allocation. The pri-

oritization scheme will allow robots to minimize the control effort expenditure as they move within the set \mathcal{V} . We describe the methodology in the following section.

3 Methodology

We propose to leverage the environmental dynamics and the inherent environmental noise to synthesize energy-efficient control policies for a team of mobile sensing resources/robots to maintain the desired allocation in \mathcal{W} at all times. We assume each robot has a map of the environment. In our scenario, this assumption translates to providing the robots knowledge of LCS boundaries that define each V_i in \mathcal{G} . While this assumption may seem unrealistic, since LCS curves separate \mathcal{W} into regions with distinct flow dynamics, this is analogous to providing autonomous ground or aerial vehicles with a map of the environment which is often obtained *a priori*. In a fluidic environment, the map can be obtained by locating the maximum FTLE ridges based on historical data and tracking these boundaries, potentially in real-time, using a strategy similar to the one found in Hsieh et al. (2012). Thus, we assume each robot has a map of the environment and has the ability to determine the direction it is moving in within the global coordinate frame, *i.e.*, the ability to localize.

3.1 Controller Synthesis

Consider a team of N robots initially distributed across M gyres/cells. Since the objective is to achieve a desired allocation of $\tilde{\mathbf{N}}$ at all times, the proposed strategy will consist of two phases: an auction to determine which robots within each V_i should be tasked to leave/stay and an actuation phase where robots execute the appropriate leave/stay controller.

3.1.1 Auction Phase

The purpose of the auction phase is to determine whether $N_i(t) > \tilde{N}_i$ and to assign the appropriate actuation strategy for each robot within V_i . Let Q_i denote an ordered set whose elements provide robot identities that are arranged from highest escape likelihoods to lowest escape likelihoods from V_i .

In general, to first order we assume a geometric measure whereby the escape likelihood of any particle within V_i increases as it approaches the boundary of V_i , denoted as ∂V_i (Forgoston et al., 2011). Given \mathcal{W} , with dynamics given by (2), consider the case when $\varepsilon = 0$ and $I \neq 0$, *i.e.*, the case when the fluid dynamics is time independent in the presence of noise. The boundaries between each V_i are given by the stable and unstable manifolds of the saddle points within \mathcal{W} as shown in Fig. 2(a). While there exists a stable attractor in each V_i when $I = 0$, the presence of noise means that robots originating in V_i have a non-zero probability of landing in a neighboring gyre V_j where $e_{ij} \in \mathcal{E}$. Here we assume that robots experience the same escape likelihoods in each

gyre/cell and assume that $P_k(\neg i|i)$, the probability that a robot escapes from region i to an adjacent region, can be estimated based on a robot's proximity to a cell boundary with some assumption of the environmental noise profile (Forgoston et al., 2011).

In other words, $Q_i = \{k_1, \dots, k_{N_i}\}$ such that $\|q_{k_1} - \partial V_i\|_\infty \leq \|q_{k_2} - \partial V_i\|_\infty \leq \dots \leq \|q_{N_i} - \partial V_i\|_\infty$ where $\|\cdot\|_\infty$ denotes the infinity norm. The set Q_i provides the prioritization scheme for tasking robots within V_i to leave if $N_i(t) > \bar{N}_i$. The assumption is that robots with higher escape likelihoods are more likely to be “pushed” out of V_i by the environment dynamics and will not have to exert as much control effort when moving to another cell, minimizing the overall control effort required by the team.

In general, a simple auction scheme can be used to determine Q_i in a distributed fashion by the robots in V_i (Dias et al., 2006). If $N_i(t) > \bar{N}_i$, then the first $N_i - \bar{N}_i$ elements of Q_i , denoted by $Q_{iL} \subset Q_i$, are tasked to leave V_i . The number of robots in V_i can be established in a distributed manner in a similar fashion. The auction can be executed periodically at some frequency $1/T_a$ where T_a denote the length of time between each auction and should be greater than the relaxation time of the AUV/ASV dynamics. This step is summarized in Algorithm 1.

Algorithm 1 Auction Phase

```

1: if ElapsedTime ==  $T_a$  then
2:   Execute auction and determine  $N_i(t)$  and  $Q_i$ 
3:   if  $N_i(t) > \bar{N}_i$  then
4:     if  $k \in Q_L$  then
5:        $u_k \rightarrow U_L \forall k \in Q_L$ 
6:     else
7:        $u_k \rightarrow U_S$ 
8:     end if
9:   else
10:     $u_k \rightarrow U_S \forall k \in Q_i$ 
11:   end if
12: end if

```

3.1.2 Actuation Phase

For the actuation phase, individual robots execute their assigned controllers depending on whether they were tasked to stay or leave during the auction phase. As such, the individual robot control strategy is a hybrid control policy consisting of three discrete states: a leave state, U_L , and two stay states, U_{SA} and U_{SP} . Robots who are tasked to leave will execute U_L until they have left V_i or until they have been once again tasked to stay. Robots who are tasked to stay will execute U_{SP} if $\|q_{k_1} - \partial V_i\|_\infty > d_{min}$ and U_{SA} otherwise. In other words, if a robot's distance to the cell boundary is below some minimum threshold distance d_{min} , then the robot will actuate and move itself away from the boundary of V_i . If a robot's distance to ∂V_i is above d_{min} , then the robot

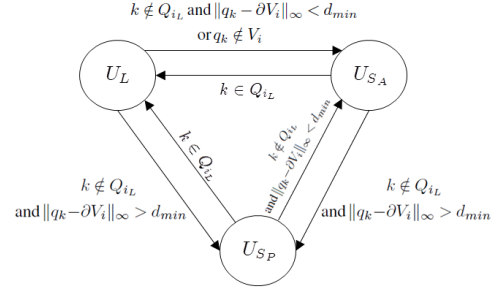


Fig. 3. Schematic of the single-robot hybrid robot control policy.

will execute no control actions. Robots will execute U_{SA} until they have reached a state where $\|q_{k_1} - \partial V_i\|_\infty > d_{min}$ or until they are tasked to leave at a later auction round. Similarly, robots will execute U_{SP} until either $\|q_{k_1} - \partial V_i\|_\infty \leq d_{min}$ or they are tasked to leave. The hybrid robot control policy is given by

$$U_L(\mathbf{q}_k) = \omega_i \times c \frac{F(\mathbf{q}_k)}{\|F(\mathbf{q}_k)\|}, \quad (3a)$$

$$U_{SA}(\mathbf{q}_k) = -\omega_i \times c \frac{F(\mathbf{q}_k)}{\|F(\mathbf{q}_k)\|}, \quad (3b)$$

$$U_{SP}(\mathbf{q}_k) = 0. \quad (3c)$$

Here, $\omega_i = [0, 0, 1]^T$ denotes counterclockwise rotation with respect to the center of V_i , with clockwise rotation being denoted by the negative and c is a constant that sets the linear speed of the robots. The hybrid control policy generates a control input perpendicular to the fluid velocity measured by robot k and pushes the robot away from the center of V_i if U_L is selected, towards the center of V_i if U_{SA} is selected, or results in no control input if U_{SP} is selected. The hybrid control policy is summarized in Fig. 3.

In general, the Auction Phase is executed at a frequency of $1/T_a$ which means robots also switch between controller states at a frequency of $1/T_a$. To further reduce actuation efforts exerted by each robot, it is possible to limit a robot's actuation time to a period of time $T_c \leq T_a$. Such a scheme may prolong the amount of time required for the team to achieve the desired allocation, but may result in significant energy-efficiency gains. We further analyze the proposed strategy in the following sections.

4 Analysis

In this section, we discuss the theoretical feasibility of the proposed distributed allocation strategy. Instead of the traditional agent-based analysis, we employ a macroscopic analysis of the proposed distributed control strategy given by Algorithm 1 and (3) similar to that found in Mather and Hsieh (2011). For a team of N robots, each executing the same hybrid control strategy shown in Fig. 3, we represent the ensemble dynamics as a *polynomial stochastic hybrid system*

The system state is given by $\mathbf{N}(t) = [N_1(t), \dots, N_M(t)]^T$. As the team distributes across the M regions, the rate in which robots leave a given V_i can be modeled using constant *transition rates*. For every edge $e_{ij} \in \mathcal{E}$, we assign a constant $a_{ij} > 0$ such that a_{ij} gives the transition probability per unit time for a robot from V_i to land in V_j . Different from Mather and Hsieh (2011), the a_{ij} ’s are a function of the parameters (c , T_c , and T_a) of the individual robot control policy (3), the dynamics of the surrounding fluid, and the inherent noise in the environment. Furthermore, a_{ij} is a macroscopic description of the system and thus a parameter of the ensemble dynamics rather than the agent-based system. As such, the macroscopic analysis is a description of the steady-state behavior of the system and becomes exact as N approaches infinity.

$$N_i \xrightarrow{a_{ij}} N_j \quad \forall e_{ij} \in \mathcal{E}. \quad (4)^{365}$$

Given (4) and employing the extended generator we can obtain the following description of the moment dynamics of the system:

where $[\mathbf{A}]_{ij} = a_{ji}$ and $[\mathbf{A}]_{ii} = -\sum_{(i,j) \in \mathcal{E}} a_{ij}$ (Mather and Hsieh, 2011). It is important to note that \mathbf{A} is a Markov process matrix and thus is negative semidefinite. This coupled with the conservation constraint $\sum_i N_i = N$ leads to exponential stability of the system given by (5) (Klavins, 2010).

Theorem 1 *Given a team of N robots with kinematics given by (1) and \mathbf{v}_f given by (2), the distributed allocation strategy given by Algorithm 1 and (3), at the ensemble level is stable and achieves the desired allocation strategy.*

42	42	42	42	0	0	0	0	0	0	0	0
42	0	0	42	0	125	125	0	0	166	0	0
42	0	0	42	0	125	125	0	0	166	166	0
42	42	42	42	0	0	0	0	0	0	0	0

5 Simulation Results

We assume $N = 500$ and $T_a = 10$ and initialize the team of 500 robots randomly across the M gyres. Each simulation was performed for a long enough period of time until steady-state has been reached. We considered three different allocations across the grid of 4×4 gyres forming a Ring, a Block, and an L-Shape pattern as shown in Fig. 4. For the ring pattern, we consider the case when the actuation was applied for $T_c = fT_a$ amount of time where $f = 0.1, 0.2, \dots, 1.0$. The Block and L-Shape patterns we considered the cases when $T_c = 0.5T_a$ and $T_c = T_a$.

For time-invariant flows, we assume $\varepsilon = 0$, $A = 0.5$, $s = 20$, $\mu = 0.005$, and $I = 35$ in (2). The final population distribution of the team for the case with no controls and the cases with controls for each of the patterns are shown in Fig. 5.

For each pattern and corresponding value of T_c , we execute a total of five runs. To evaluate the performance of the proposed strategy, we compute the average root mean squared errors (RMSE) of the population differences over all $M + 1$ cells within the total space over all runs. Additionally, we consider the total control expenditure by the team. The total control expenditure is computed by integrating the magnitude of the average control velocity over time for each robot. We compare our results to a baseline deterministic allocation strategy where the desired allocation is pre-computed and individual robots follow fixed trajectories when navigating from one gyre to another. For this baseline case, robots travel in straight lines at fixed speeds using a simple PID tra-

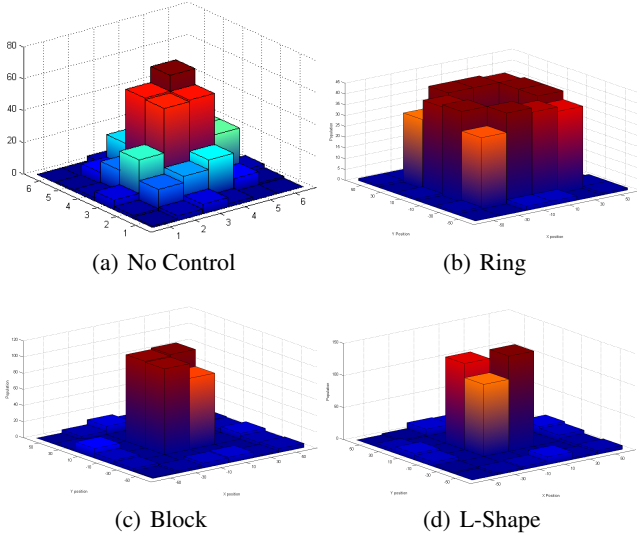


Fig. 5. Histogram of the final allocations in the time-invariant flow field for the swarm of (a) passive robots exerting no controls and robots exerting control forming the (b) Ring pattern with $T_c = 0.8T_a$ at $t = 450$, (c) Block pattern with $T_c = T_a$ at $t = 450$, and (d) L-shape pattern with $T_c = 0.5T_a$ at $t = 450$.

T_c	2	5	8	9	10	Baseline
Ring Pattern	12.99	5.98	3.45	3.49	3.66	4.09
Block Pattern	-	11.21	-	-	12.72	-
L Pattern	-	30.09	-	-	30.45	-

Table 1. Summary of RMSE's for each simulation pattern at $t=450$ with the time-invariant flow field.

jectory follower and treat the surrounding fluid dynamics as an external disturbance source. The RMSE results for all patterns are summarized in Table 1 and Figs. 6-8.

5.2 In Time-Varying Flows

For the time-varying, periodic flow, we assume $A = 0.5$, $s = 20$, $\mu = 0.005$, $I = 35$, $\rho = 2s$, $\phi = 0$ and $\psi = 0$ in (2). Additionally, we considered the performance of our control strategy for different values of ω and ε with $T_c = 8$. In all these simulations, the boundaries of each V_i is given by the FTLE ridges computed for the time-independent system. The final population distribution of the team for the case with no controls and the cases with controls for each of the patterns are shown in Fig. 9. The final population RMSE for the cases with different ω and ε values for the Ring and L-shape patterns are shown in Fig. 10. These figures show the average of 10 runs for each ω and ε pair. In each of these runs, the swarm of mobile sensors were initially randomly distributed within the grid of 4×4 cells. Finally, Fig. 11 and 12 shows the population RMSE as a function of time and the average control effort for an individual robot for the Ring and L-shape patterns respectively.

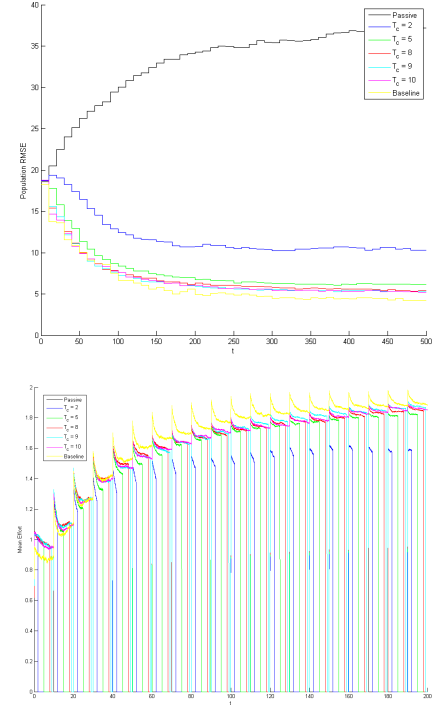


Fig. 6. Comparison of RMSE and Total Control Effort for the Ring pattern for different T_c with the baseline controller with time-invariant flows.

5.3 In Experimental Flows

Using our $0.6m \times 0.6m \times 0.3m$ experimental flow tank equipped with a grid of 4×3 set of driving cylinders, we generated a time-invariant multi-gyre flow field. Particle image velocimetry (PIV) was used to extract the surface flows at 7.5 Hz resulting in a 39×39 grid of velocity measurements. The data was collected for a total of 60 sec . Fig. shows the top view of our experimental testbed and the resulting flow field obtained via PIV. Using this data, we simulated a swarm of 500 mobile sensors executing the control strategy given by Eq. (3).

To determine the appropriate tessellation of the workspace, we averaged the positions of the LCS ridges obtained for each frame of the velocity field over time. This resulted in the discretization of the space into a grid of 4×3 cells. Each cell corresponds to a single gyre as shown Fig. 14. The cells of primary concern are the central pair and the remainder boundary cells were not used to avoid boundary effects and to allow robots to escape the center gyres in all directions. The robots were initially uniformly distributed across the two center cells and all 500 robots were tasked to stay within the upper center cell. When no control effort is exerted by the robots, the final population distribution achieved by the team is shown in Fig. 15(a). With controls, the final population distribution is shown in Fig. 15(b). The control strategy was applied assuming $T_c/T_a = 0.8$. The

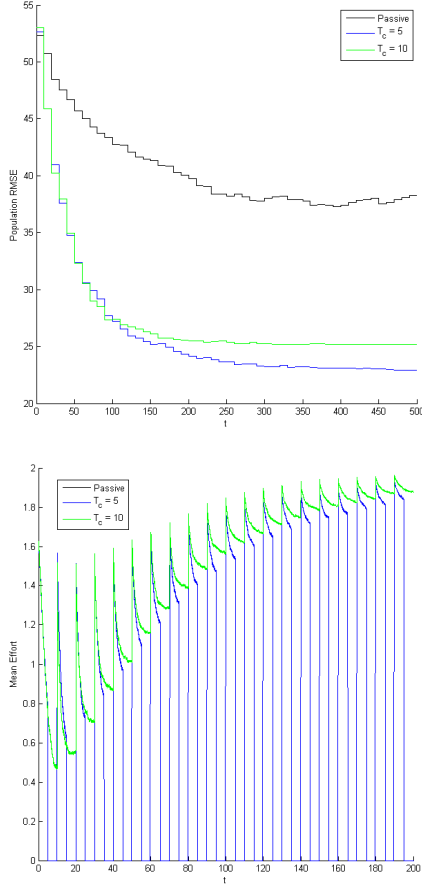


Fig. 7. Comparison of RMSE and Total Control Effort for the Block pattern for different T_c with the baseline controller with time-invariant flows.

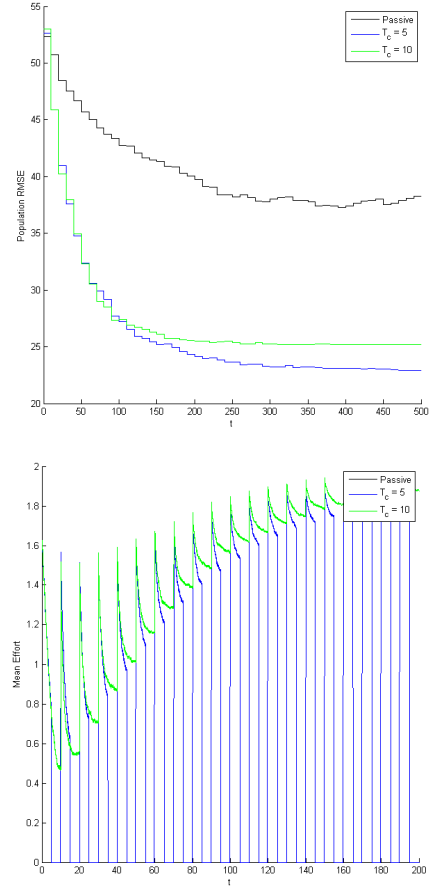


Fig. 8. Comparison of RMSE and Total Control Effort for the L-Shape pattern for different T_c with the baseline controller with time-invariant flows.

final RMSE for different values of c in Eq. (3) and T_a is shown in Fig. 16(a) and RMSE as a function of time for different values of c and T_a are shown in Fig. 16(b).

6 Discussion

In time-invariant flows, we note that for large enough T_c , our proposed distributed control strategy performs comparable to the baseline controller both in terms of steady-state error and convergence time. As T_c decreases, less and less control effort is exerted and thus it becomes more and more difficult for the team to achieve the desired allocation. This is confirmed by both the RMSE results summarized in Table 1 and Fig. 6(a)-8(a). Furthermore, while the proposed control strategy does not beat the baseline strategy as seen in Fig. 6(a), it does come extremely close to matching the baseline strategy performance, while requiring much less control effort as shown in Fig. 6(b) even at high duty cycles, *i.e.*, when $T_c/T_a > 0.5$.

More interestingly, we note that executing the proposed control strategy at 100% duty cycle, *i.e.*, when $T_c = T_a$, in

time-invariant flows did not always result in better performance. This is true for the cases when $T_c = 0.5T_a = 5$ for the Block and L-shaped patterns shown in Fig. 7(a) and 8(a). In these cases, less control effort yielded improved performance. However, further studies are required to determine the critical value of T_c when less control yields better overall performance. In time-invariant flows, our proposed controller can more accurately match the desired pattern while using approximately 20% less effort when compared to the baseline controller.

In time-varying, periodic flows we note that our proposed control strategy is able to achieve the desired final allocation even at 80% duty cycle, *i.e.*, $T_c = 0.8T_a$. This is supported by the results shown in Fig. 10. In particular, we note that the proposed control strategy performs quite well for a range of ω and ε parameters for both the Ring and L-shape patterns. While the variation in final RMSE values for the Ring pattern is significantly lower than the L-shape pattern, the variations in final RMSE values for the L-shape are all within 10% of the total swarm population.

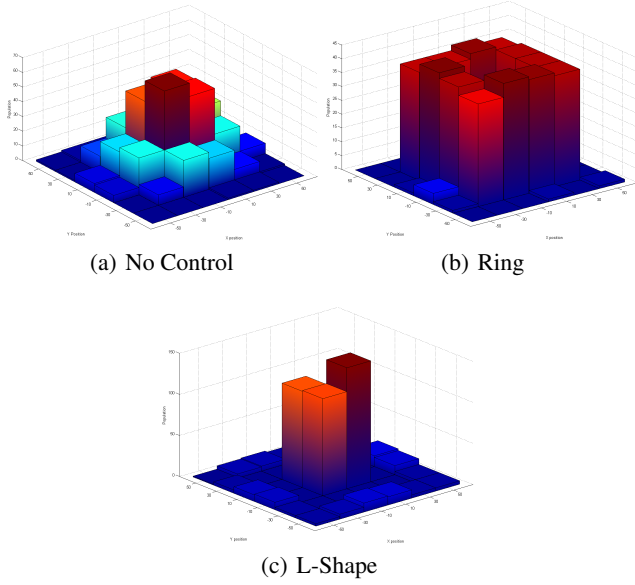


Fig. 9. Histogram of the final allocations in periodic flows, with parameters of $\omega = \frac{5\pi}{40}$ and $\varepsilon = 5$, for the swarm of (a) passive robots exerting no controls and robots exerting control forming the (b) Ring pattern with $T_c = 0.8T_a$ at $t = 450$, and (c) L-Shape pattern with $T_c = 0.5T_a$ at $t = 450$.

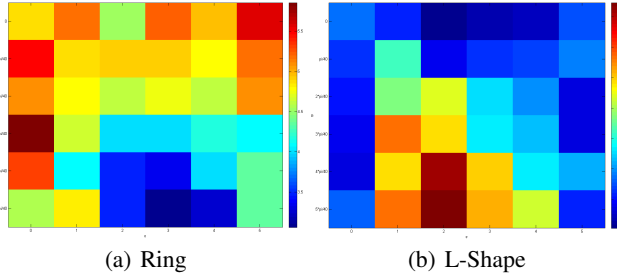


Fig. 10. Final population RMSE for different values of ω and ε with $T_c = 8$ and $d_{min} = 4$. The remaining model parameters are the same as in the time-invariant case.

Lastly, the results obtained using the experimental flow field shows that the proposed control strategy has the potential to be effective in realistic flows. However, the resulting performance will require good matching between the amount of control effort a vehicle can realistic exert, the frequency in which the auctions occur within a cell, and the time scales of the environmental dynamics as shown in in Figs. 16(a) and 16(b). This is an area for future investigation.

7 Conclusions and Future Outlook

In this work, we presented the development of a distributed hybrid control strategy for a team of robots to maintain a desired spatial distribution in a stochastic geophysical fluid en-

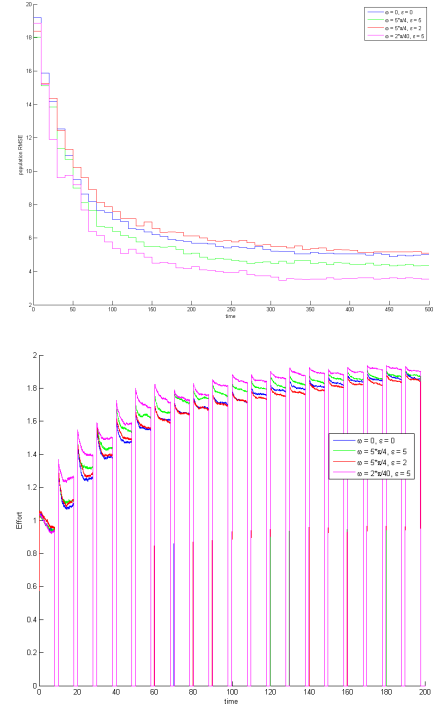


Fig. 11. Comparison of RMSE and Control Effort over time for select ω and ε pairs for the Ring pattern in periodic flows.

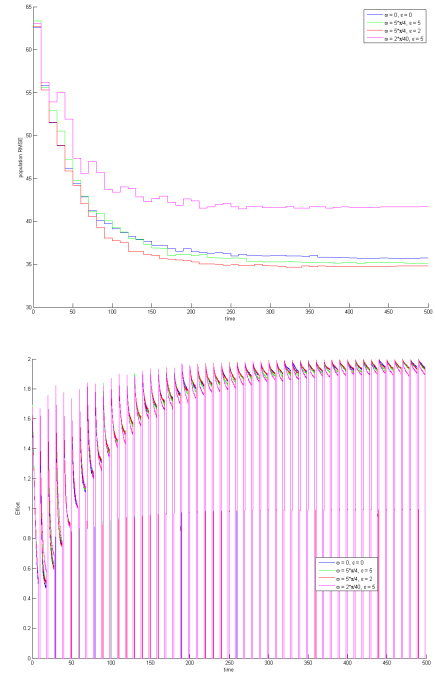
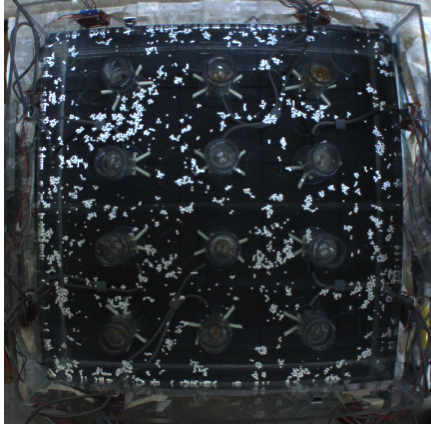
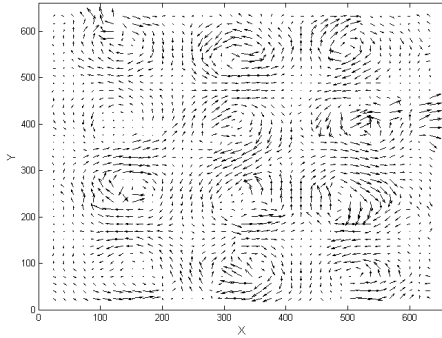


Fig. 12. Comparison of RMSE and Control Effort over time for select ω and ε pairs for the L-shape pattern in periodic flows.



(a)



(b)

Fig. 13. (a) Experimental setup of flow tank with 12 driven cylinders. (b) Flow field for image (a) obtained via particle image velocimetry (PIV).

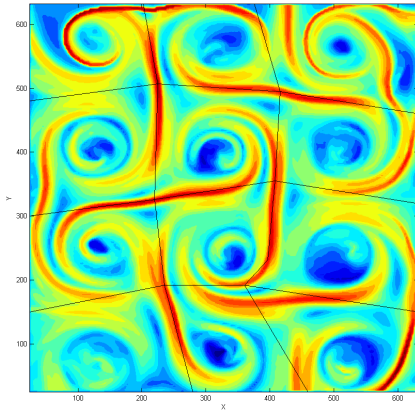
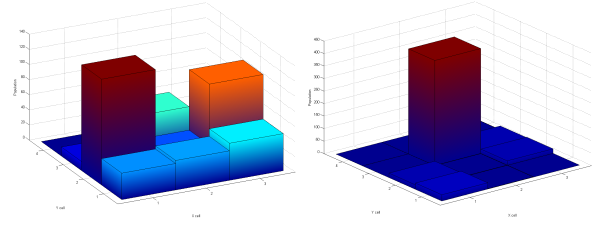


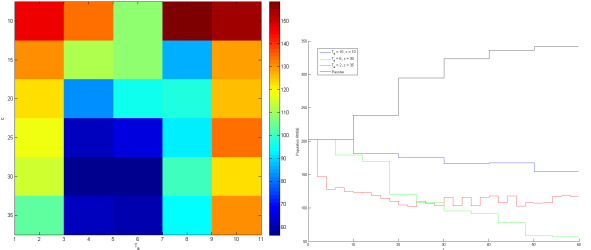
Fig. 14. FTLE field for the mean of the experimental data set over time. The field is discretized into a grid of 4×3 cells whose boundaries are shown in black.



(a)

(b)

Fig. 15. Population distribution for a swarm of 500 mobile sensors over a period of 60 sec (a) with no controls, *i.e.*, passive, and (b) with controls.



(a)

(b)

Fig. 16. (a) Final RMSE for different values of c (Eq. 3) and T_a using the experimental flow field. $T_c/T_a = 0.8$ is kept constant throughout. (b) RMSE over time for select c and T_a parameters on an experimental flow field. The duty cycle $T_c/T_a = 0.8$ is kept constant throughout.

environment. We assumed robots have a map of the workspace which in the fluid setting is akin to having some estimate of the global fluid dynamics. This can be achieved by knowing the locations of the material lines within the flow field that separate regions with distinct dynamics. Using this knowledge, we leverage the surrounding fluid dynamics and inherent environmental noise to synthesize energy efficient control strategies to achieve a distributed allocation of the team to specific regions in the workspace. Our initial results show that using such a strategy can yield similar performance as deterministic approaches that do not explicitly account for the impact of the fluid dynamics while reducing the control effort required by the team.

For future work we are interested in using actual ocean flow data to further evaluate our distributed allocation strategy. Specifically, we are interested in using more complicated flow models including a bounded single-layer PDE ocean model (Forgoston et al., 2011), a multi-layer PDE ocean model (Wang et al., 2009; Lolla et al., 2012), and realistic 2D and 3D unbounded flow models provided by the Navy Coastal Ocean Model (NCOM) database. Particularly, we are interested in extending our strategy to non-periodic, time-varying flows. In addition, we are currently developing an experimental testbed capable of generating complex 2D flows in a controlled laboratory setting. The objective is to

be able to evaluate the proposed control strategy using experimentally generated flow field data whose dynamics are similar to realistic ocean flows. Finally, since our proposed strategy requires robots to have some estimate of the global fluid dynamics, another immediate direction for future work is to determine how well one can estimate the fluid dynamics given knowledge of the locations of Lagrangian coherent structures (LCS) in the flow field.

Acknowledgements. KM and MAH were supported by the Office of Naval Research (ONR) Award No. N000141211019. EF was supported by the U.S. Naval Research Laboratory (NRL) Award No. N0017310-2-C007. IBS was supported by ONR grant N0001412WX20083 and the NRL Base Research Program N0001412WX30002. The authors additionally acknowledge support by the ICMAT Severo Ochoa project SEV-2011-0087.

References

- Berman, S., Halasz, A., Hsieh, M. A., and Kumar, V.: Navigation-based Optimization of Stochastic Deployment Strategies for a Robot Swarm to Multiple Sites, in: Proc. of the 47th IEEE Conference on Decision and Control, Cancun, Mexico, 2008.
- Caron, D., Stauffer, B., Moorthi, S., Singh, A., Batalin, M., Graham, E., Hansen, M., Kaiser, W., Das, J., de Menezes Pereira, A., A. Dhariwal, B. Z., Oberg, C., and Sukhatme, G.: Macro to fine-scale spatial and temporal distributions and dynamics of phytoplankton and their environmental driving forces in a small subalpine lake in southern California, USA, *Journal of Limnology and Oceanography*, 53, 2333–2349, 2008.
- Chen, V., Batalin, M., Kaiser, W., and Sukhatme, G.: Towards Spatial and Semantic Mapping in Aquatic Environments, in: IEEE International Conference on Robotics and Automation, pp. 629–636, Pasadena, CA, 2008.
- Dahl, T. S., Mataric, M. J., and Sukhatme, G. S.: A machine learning method for improving task allocation in distributed multi-robot transportation, in: *Understanding Complex Systems: Science Meets Technology*, edited by Braha, D., Minai, A., and Bar-Yam, Y., pp. 307–337, Springer, Berlin, Germany, 2006.
- Das, J., Py, F., Maughan, T., O'Reilly, T., Messie, M., J. Ryan, G. S., and Rajan, K.: Simultaneous Tracking and Sampling of Dynamic Oceanographic Features with AUVs and Drifters, Submitted to *International Journal of Robotics Research*, 2011.
- DeVries, L. and Paley, D. A.: Multi-vehicle control in a strong flow-field with application to hurricane sampling, Accepted for publication in the *AIAA J. Guidance, Control, and Dynamics*, 2011.
- Dias, M. B., Zlot, R. M., Kalra, N., and Stentz, A. T.: Market-based multirobot coordination: a survey and analysis, *Proceedings of the IEEE*, 94, 1257–1270, 2006.
- Forgoston, E., Billings, L., Yecko, P., and Schwartz, I. B.: Set-based corral control in stochastic dynamical systems: Making almost invariant sets more invariant, *Chaos*, 21, 2011.
- Gerkey, B. P. and Mataric, M. J.: Sold!: Auction methods for multi-robot control, *IEEE Transactions on Robotics & Automation*, 18, 758–768, 2002.
- Gerkey, B. P. and Mataric, M. J.: A Formal Framework for the Study of Task Allocation in Multi-Robot Systems, *International Journal of Robotics Research*, 23, 939–954, 2004.
- Haller, G.: A variational theory of hyperbolic Lagrangian Coherent Structures, *Physica D*, 240, 574–598, 2011.
- Haller, G. and Yuan, G.: Lagrangian coherent structures and mixing in two-dimensional turbulence, *Phys. D*, 147, 352–370, doi:10.1016/S0167-2789(00)00142-1, <http://dl.acm.org/citation.cfm?id=366463.366505>, 2000.
- Hsieh, M. A., Halasz, A., Berman, S., and Kumar, V.: Biologically inspired redistribution of a swarm of robots among multiple sites, *Swarm Intelligence*, 2008.
- Hsieh, M. A., Forgoston, E., Mather, T. W., and Schwartz, I. B.: Robotic Manifold Tracking of Coherent Structures in Flows, in: in the Proc. of the IEEE International Conference on Robotics and Automation, Minneapolis, MN USA, 2012.
- Inanc, T., Shadden, S., and Marsden, J.: Optimal trajectory generation in ocean flows, in: *American Control Conference*, 2005. Proceedings of the 2005, pp. 674 – 679, doi:10.1109/ACC.2005.1470035, 2005.
- Klavins, E.: Proportional-Integral Control of Stochastic Gene Regulatory Networks, in: Proc. of the 2010 IEEE Conf. on Decision and Control (CDC2010), Atlanta, GA USA, 2010.
- Lolla, T., Ueckermann, M. P., Haley, P., and Lermusiaux, P. F. J.: Path Planning in Time Dependent Flow Fields using Level Set Methods, in: in the Proc. IEEE International Conference on Robotics and Automation, Minneapolis, MN USA, 2012.
- Lynch, K. M., Schwartz, I. B., Yang, P., and Freeman, R. A.: Decentralized environmental modeling by mobile sensor networks, *IEEE Trans. Robotics*, 24, 710–724, 2008.
- Mather, T. W. and Hsieh, M. A.: Distributed Robot Ensemble Control for Deployment to Multiple Sites, in: *2011 Robotics: Science and Systems*, Los Angeles, CA USA, 2011.
- Senatore, C. and Ross, S.: Fuel-efficient navigation in complex flows, in: *American Control Conference*, 2008, pp. 1244 –1248, doi:10.1109/ACC.2008.4586663, 2008.
- Shadden, S. C., Lekien, F., and Marsden, J. E.: Definition and properties of Lagrangian coherent structures from finite-time Lyapunov exponents in two-dimensional aperiodic flows, *Physica D: Nonlinear Phenomena*, 212, 271 – 304, doi:DOI: 10.1016/j.physd.2005.10.007, <http://www.sciencedirect.com/science/article/pii/S0167278905004446>, 2005.
- Sydney, N. and Paley, D. A.: Multi-vehicle control and optimization for spatiotemporal sampling, in: *IEEE Conf. Decision and Control*, pp. 5607–5612, Orlando, FL, 2011.
- Wang, D., Lermusiaux, P. F., Haley, P. J., Eickstedt, D., Leslie, W. G., and Schmidt, H.: Acoustically focused adaptive sampling and on-board routing for marine rapid environmental assessment, *Journal of Marine Systems*, 78, 393–407, 2009.
- Williams, R. and Sukhatme, G.: Probabilistic Spatial Mapping and Curve Tracking in Distributed Multi-Agent Systems, in: Submitted to *IEEE International Conference on Robotics and Automation*, Minneapolis, MN, 2012.
- Wu, W. and Zhang, F.: Cooperative Exploration of Level Surfaces of Three Dimensional Scalar Fields, *Automatica, the IFAC Journal*, 47, 2044–2051, 2011.
- Zhang, F., Fratantoni, D. M., Paley, D., Lund, J., and Leonard, N. E.: Control of Coordinated Patterns for Ocean Sampling, *International Journal of Control*, 80, 1186–1199, 2007.